ELSEVIER

International Journal of Heat and Fluid Flow 20 (1999) 26–33

International Journal of
HEAT AND
FLUID FLOW

Flow of a stratified fluid in a cylinder with a rotating lid

Chang Ho Lee, Jae Min Hyun *

Department of Mechanical Engineering, Korea Advanced Institute of Science and Technology, 373-1 Kusong-Dong, Yusungku, Taejon, 305-701, South Korea

Received 17 March 1998; accepted 21 July 1998

Abstract

A numerical study is made for the flow of a density-stratified fluid in a vertical cylinder with a rotating top lid. Under the Boussinesq-fluid assumption, the governing Navier–Stokes equations are numerically solved. For large rotational Reynolds number Re and the cylinder aspect ratio A $\sim$ O(1), details of flow and temperature fields are displayed. The effect of the Prandtl number on global flow patterns is scrutinized for both gravitationally unstable and gravitationally stable configurations. Of particular interest is the behavior of the vortex breakdown stagnation bubble under the influence of buoyancy. Plots are presented for the azimuthal vorticity fields, in line with the simple axisymmetric inviscid kinematic consideration. An explicit comparison is made for the individual terms appearing in the azimuthal vorticity equation. For both gravitationally unstable and gravitationally stable configurations, the argument based on the behavior of azimuthal vorticity is seen to produce predictions consistent with the numerical results.

1. Introduction

The motion of a viscous fluid contained in a closed vertically mounted cylindrical vessel, with a rotating endwall disk lid, poses an attractive example of confined swirling flow. The major flow characteristics are known to be determined by two nondimensional parameters, i.e., the rotational Reynolds number $\mathrm{Re} \equiv \Omega R^2/\nu$, and aspect ratio of the cylinder $A \equiv H/R$, in which the cylinder radius is R, cylinder height H, rotation rate of the lid Ω, and kinematic viscosity of the fluid ν, respectively. Flows of technological relevance are typically in the range $\mathrm{Re} \gg 1$ and $A \sim \mathrm{O}(1)$.

The overall flow patterns are such that the dominant velocity component is in the azimuthal direction. However, it is noted that meridional flows of varying character, although small in magnitude, are induced, and the physical implications of these meridional flows are complex and far-reaching. For a constant-density fluid, systematic experiments were conducted by Escudier (1984) to visualize the salient features of meridional flows as both Re and A encompass practically attainable and dynamically meaningful ranges. As well documented, the global meridional flow structure is characterized by the presence of Ekman boundary layers on the endwall disks, and, in the interior core, an axial motion principally in the direction toward the rotating disk exists. This produces general meridional circulation patterns, and the return circuit is carried via sidewall boundary layers adjacent to the cylindrical wall. This paradigmatic picture has been verified in preceding experimental and numerical investigations [e.g., Pao, 1970, 1972; Bertela and Gori, 1982; Escudier, 1984].

For $A \gtrsim 1.20$ and $\mathrm{Re} \gtrsim 1020$, significant structural changes are seen to take place in the above-illustrated meridional circulation patterns. With a proper combination of A and Re, the meridional motion in the vicinity of the axis ceases to be monotonic; stagnation points occur on the axis, accompanied by a closed stream surface, which leads to a stagnation bubble. This phenomenon has been interpreted to be a manifestation of the celebrated vortex breakdown, which has been observed in a number of seemingly different flow conditions [e.g., Escudier, 1986, 1988]. By a meticulous experimental program, Escudier (1984) constructed a Re–A diagram, identifying the parameter space in which the above-described vortex breakdown has been observed to occur.

Efforts to gain a fundamental understanding of the appearance of the stagnation bubble and, in a broader context, attempts to ascertain the dynamic mechanism of vortex breakdown phenomenon have been reported in the literature. Several descriptive arguments have been advanced, however, as remarked by Brücker and Althaus (1995), physically convincing explanations on the basic nature of vortex breakdown have yet to be refined. Lopez (1990) and Brown and Lopez (1990), by examining the detailed numerical solutions, devised a simplified analytic model to illuminate the physical mechanisms for vortex breakdown. For $\mathrm{Re} \gg 1$, they proposed an approximate approach to explore the physical mechanism for vortex breakdown by using a simplistic, steady, inviscid axisymmetric equation of motion. The key element of their endeavor lies in examining directly, not through perturbations of an initial stream function, the behavior of azimuthal vorticity. Lopez (1990) and Brown and Lopez (1990) clearly demonstrated that their criterion for vortex breakdown, which is based on the generation of negative azimuthal vorticity on some stream surfaces, leads to consistent results in predicting

* Corresponding author. E-mail: jmhyun@cais.kaist.ac.kr

0142-727X/99/$ – see front matter
PII: S0142-727X(98)10041-3

the occurrence of breakdown bubbles. These inviscid predictions were also compared favorably against the numerical solutions of the full Navier–Stokes equations as well as the visualizations (Escudier, 1984) for which breakdown occurs. More recently, the validity of these theoretical reasonings suggested by Brown and Lopez was positively tested by particle-tracking velocimetry data of Brücker and Althaus (1995).

It is important to notice that the majority of previous investigations have dealt with the case of a homogeneous fluid. Depictions of the flow field of a density-stratified fluid, with substantial buoyancy effects, have not been addressed in sufficient detail. Since buoyancy directly affects the vertical flow, and, therefore, the meridional motion in general, the axial (vertical) flow structure and the behavior of the attendant stagnation bubble are anticipated to be significantly altered by the introduction of nonhomogeneity of density field. Lugt and Abboud (1987) secured numerical solutions to the axisymmetric Navier–Stokes equations using a Boussinesq-fluid, with the temperature at the bottom stationary endwall disk higher than that at the top rotating disk. The vertical sidewall was thermally insulated. This configuration represents an overall unstable stratification, and only the results of a small selected number of exemplary cases were presented. Numerically obtained global fields of meridional flows and isotherm contours were illustrated, and these led to the observation that the occurrence and properties of the stagnation bubble are strongly influenced by the buoyancy effect. However, in the numerical account of Lugt and Abboud (1987), no detailed explorations were made into the physical mechanisms of the changes in meridional flow and in vortex breakdown phenomenon. As remarked by Brown and Lopez (1990), no specific information was offered in Lugt and Abboud (1987) on the distribution of azimuthal vorticity, among others, which would help explain the dynamics pertinent to the development of stagnation bubble.

Recently, Kim and Hyun (1997) produced numerical solutions to the governing Navier–Stokes equations when the overriding stratification is stable, i.e., the temperature at the top rotating lid, T_T is higher than that at the bottom stationary lid, T_L. The focus was to describe the alterations in meridional flow patterns as the rotational effect, which is denoted by the afore-defined Reynolds number Re, and the buoyancy effect compete for the control of interior flow. The additional nondimensional parameter for this purpose is the Richardson number $\mathrm{Ri} \equiv g\beta\Delta T/R\Omega^2$, where g is gravity, β the coefficient of thermometric expansion of the fluid, ΔT the imposed temperature difference between the top and bottom lids, i.e., $\Delta T \equiv T_T - T_L$. The stagnation bubble, which forms when Re is very large, disappears when $\mathrm{Ri} \gtrsim \mathrm{O}(1)$, since, under substantial stabilizing buoyancy effects, vertical velocities are suppressed. Radial profiles of local heat transfer coefficients at the lids were plotted, and the impacts of rotation and of buoyancy were scrutinized. However, in Kim and Hyun (1997), the parameter spaces for numerical calculations were limited, and, more importantly, no attempts were made to ascertain the behavior of vortex breakdown as the buoyancy effect becomes substantial.

The present study is motivated by the above-stated unfulfilled tasks. Emphasis is placed on gaining further insight into the depiction and possible explanation of the behavior of meridional flows, in particular, the stagnation bubble, under buoyancy effect. Specifically, the numerical solutions will be examined in a manner similar to the juxtaposition of Lopez (1990) and Brown and Lopez (1990). Attention will be directed to the question of whether the simplified inviscid analyses of Brown and Lopez for a homogeneous fluid can be extended, with modification, to the stratified flow in hand. To this end, axial-plane contour maps of the azimuthal vorticity will be scrutinized, and the qualitative validity of the theoretical prediction of Brown and Lopez will be appraised with respect to its explanation on the formation of stagnation bubble.

2. The model

As stated, a Boussinesq fluid, which satisfies the relationship $\rho = \rho_L[1 - \beta(T - T_L)]$, where ρ and T refer to density and temperature, respectively, fills the closed cylindrical container. The motion is generated by the steady rotation of the top lid as sketched in Fig. 1. The physical properties of the fluid, such as the dynamic viscosity $\mu[\equiv \rho_L \nu]$, specific heat C_p and thermal diffusivity κ are taken to be constant. The governing axisymmetric Navier–Stokes equations in nondimensional form, expressed in cylindrical frame (r,ϕ,z) with corresponding velocity components (u,v,w), are well known [e.g., see Lugt and Abboud, 1987], and they will not be reproduced here. Nondimensionalization is performed by adopting R, $R\Omega$ and $\rho_L \times (R\Omega)^2$ for scales of length, velocity and pressure, respectively. The dimensionless temperature θ is defined as $\theta \equiv (T - T_L)/\Delta T$.

The numerical solution procedure selected here is based on the widely used SIMPLER algorithm (Patankar, 1980), in conjunction with the QUICK scheme (Hayase et al., 1994). The entire numerical solution techniques represent an expanded version of the earlier numerical investigations of Kim and Hyun (1997), which displayed broad consistency with the published results (e.g., Lugt and Abboud, 1987).

The mesh was stretched to cluster grid points near the boundaries of the computational domain. The grid network was designed such that seven grid points were placed inside the Ekman layers. For the majority of calculations, the (60×90) grid in the $(r–z)$ plane was deployed. Convergence was declared when the maximum relative difference between successive iteration steps fell below 10^{-6}. Extensive grid convergence tests were carried out. For several typical parameter sets, more refined grids were utilized to ascertain the grid-independent results. For example, the maximal relative discrepancy in the values of meridional stream function was less than 1% between

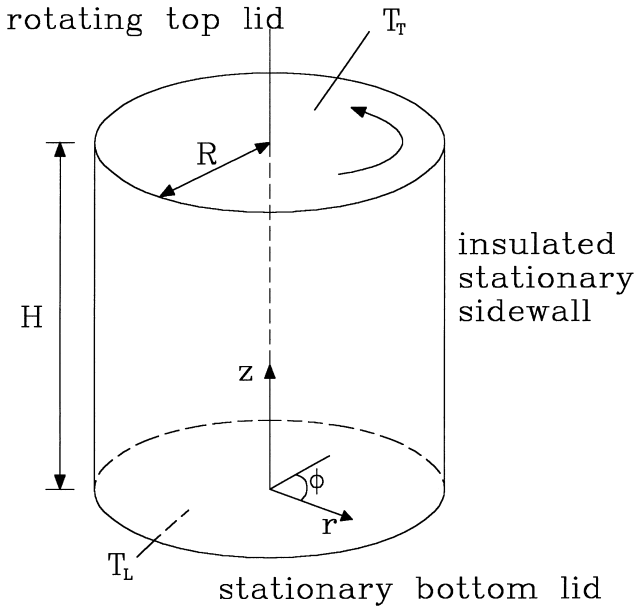

Fig. 1. Geometry and coordinate system.

the (60×90) and (99×150) grids. These tests established the reliability and accuracy of the present numerical procedures.

3. Results and discussion

Before proceeding further, it is useful to describe, in physical terms, the qualitative dynamical ingredients in the general flow situations which are relevant to vortex breakdown. For the purpose of explanation, the aspect ratio A is fixed, e.g., $A = 2.0$, and Re is increased. Due to the rotation of the top lid, in the bulk of interior core, a generally upward motion prevails, and in the sidewall boundary layer, a downward flow exists to maintain mass continuity. Near the bottom corner $(r = 1, z = 0)$, the downward flow meets the bottom stationary disk, turns in the radially inward direction in the bottom Ekman layer, and finally moves upward at small and moderate radii to fill the interior core. When Re is low, the flow in the central bottom region is monotonic owing to comparatively large viscous effects. However, when Re exceeds a threshold value, a different picture emerges. In comparative terms, the azimuthal velocity v in the central region, as the fluid leaves out of the bottom Ekman layer, is strengthened whereas the meridional flow weakens near the axis. This produces diverging helical streamlines, which in turn gives rise to a pressure increase at the axis, thereby creating an environment favorable for the appearance of a stagnation bubble. Alternatively, the combination of a smaller w and a larger v increases the local swirl angle $\phi = \arctan(v/w)$ near the axis. The crux of this argument is that, if ϕ exceeds a certain value, the pressure increase at the axis due to diverging helical streamlines leads to the situation whereby w becomes zero and negative in a certain region locally. This indicates the formation of a stagnation bubble. It is emphasized here that the interplay among the above dynamical elements is extremely subtle and delicate. When Re is too large, the relative increase in magnitude of w is bigger than that of v, implying that the divergence of helical streamlines is not sufficient to cause the formation of a stagnation bubble. In summary, vortex breakdown phenomenon, which is manifested in the presence of stagnation bubble on the axis, can be explained by the behavior of v and its interaction with the meridional flows in the interior core at small radii.

3.1. Under a gravitationally unstable temperature contrast (Ri < 0).

A limited number of numerical solutions for a gravitationally unstable configuration, [Ri < 0], i.e., when $T_T < T_L$, were examined by Lugt and Abboud (1987). It was shown that the size of stagnation bubble grows when |Ri| is small and $Pr \ll 1$. It is worth mentioning that, unless |Ri| is very small, no steady-state solutions are obtained, and this tends to restrict further the range of |Ri| in simulating flows with gravitationally unstable configuration.

An exemplary set of results, illustrating the impact of Pr, is displayed in Fig. 2 for $Re = 1600$, $A = 2.0$, $Ri = -0.01$, showing the meridional stream function ψ, θ, and curvature term v^2/r. Here, ψ is defined such that

$$u = \frac{1}{r}\frac{\partial \psi}{\partial z}, \quad w = -\frac{1}{r}\frac{\partial \psi}{\partial r}.$$

Consistent with the regime diagram of Escudier for a homogeneous fluid (Ri = 0), at this combination of Re and A, a stagnation bubble is discernible on the rotation axis [see Fig. 2(a)]. For a stratified fluid, when Pr is small, the size of the bubble is seen to be larger than for a homogeneous fluid. Until Pr reaches O(1), the bubble grows in size. However, when Pr is very large, the bubble disappears, as depicted in Fig. 2(d). These observations are in close agreement with the assertions of Lugt and Abboud.

The temperature fields are revealing. When Pr is small, much of the flow region is dominated by conduction. Therefore, the temperature distribution is close to a linear profile in the vertical direction, which, in this case, gives rise to gravitationally destabilizing buoyancy. Consequently, the meridional flows are generally intensified. However, when Pr is large, the interior flow is controlled by convection, which yields a nearly uniform temperature in the bulk of the interior; the effective buoyancy in the core is very weak. Thin boundary layer-type regions are seen adjacent to the endwall disks to accommodate the imposed temperature conditions.

In order to gain an understanding of the dynamics, the azimuthal vorticity $\eta[\equiv \partial u/\partial z - \partial w/\partial r]$ is plotted in Fig. 3. In a comprehensive discussion on the dynamic condition leading to the formation of stagnation bubble (s) for a homogeneous fluid, Lopez (1990) and Brown and Lopez (1990) emphasized the significance of the behavior of η, especially in the neighborhood of the axis. They made a thorough analysis of the velocity field induced by vorticity in the context of inviscid equations. It was ascertained that, for a stagnation bubble to occur, negative values of η are needed on some stream surfaces in the meridional plane. Lopez (1990) argued that negative values of η give rise to wavy structure of meridional flows as a preliminary process to produce a stagnation bubble. Specifically, the axial velocity w on the axis can be expressed by use of η (see Brown and Lopez, 1990):

$$w(0,z) = \frac{1}{2}\int_{-\infty}^{\infty}\int_{0}^{\infty} \frac{r^2\eta(r,z')}{[r^2 + (z-z')^2]^{3/2}}\,\mathrm{d}r\,\mathrm{d}z'. \tag{1}$$

Obviously, in order to have a negative value of $w(0,z)$, which leads to the occurrence of stagnation bubble, it is necessary to have negative values of η somewhere in the flow field. Furthermore, since $w(0,z)$ is acquired through the above integral relations, a negative value of $w(0,z)$ is more likely to be realized if η takes negative values in wider regions of flow field. This assertion, which is based on inviscid kinematic consideration, was a corner stone in the far-reaching numerical analysis of Lopez (1990) and Brown and Lopez (1990) for a homogeneous fluid. The η-plots exhibited in Fig. 3 for a stratified fluid are largely in accord with the above findings of Lopez and Brown. It is evident in Fig. 3 that larger negative values of η are seen in broader areas when the stagnation bubble is present than when no stagnation bubble occurs.

In an effort to examine in detail the mechanism of vortex breakdown, it is advantageous to gauge the relative magnitudes of individual terms in the azimuthal vorticity equation, as shown in Fig. 4.

$$\frac{\partial \eta}{\partial t} = \underbrace{-u\left(\frac{\partial \eta}{\partial r} - \frac{\eta}{r}\right) - w\frac{\partial \eta}{\partial z}}_{\text{(I)}} + \underbrace{2\frac{v}{r}\frac{\partial v}{\partial z}}_{\text{(II)}} + \underbrace{\frac{1}{\mathrm{Re}}\left[\frac{\partial}{\partial r}\left(\frac{\partial}{r\,\partial r}\right) + \frac{\partial^2 \eta}{\partial z^2}\right]}_{\text{(III)}} - \underbrace{\mathrm{Ri}\frac{\partial \theta}{\partial r}}_{\text{(IV)}}. \tag{2}$$

First, for a homogeneous fluid [θ = const., (IV) = 0], the nonlinear advection (I) takes comparatively large values in the upstream region of the stagnation bubble. As can be inferred from the plot of v^2/r of Fig. 2, the radially inward flows in the interior core yield large angular velocities since angular momentum is conserved in inviscid environment. Therefore, the principal balance is between (I) and the azimuthal velocity shear term (II) in the bulk of the interior. The viscous term (III) is substantially smaller than (I) and (II), and, expectedly, (III) becomes moderate locally in the vicinity of the bubble. It

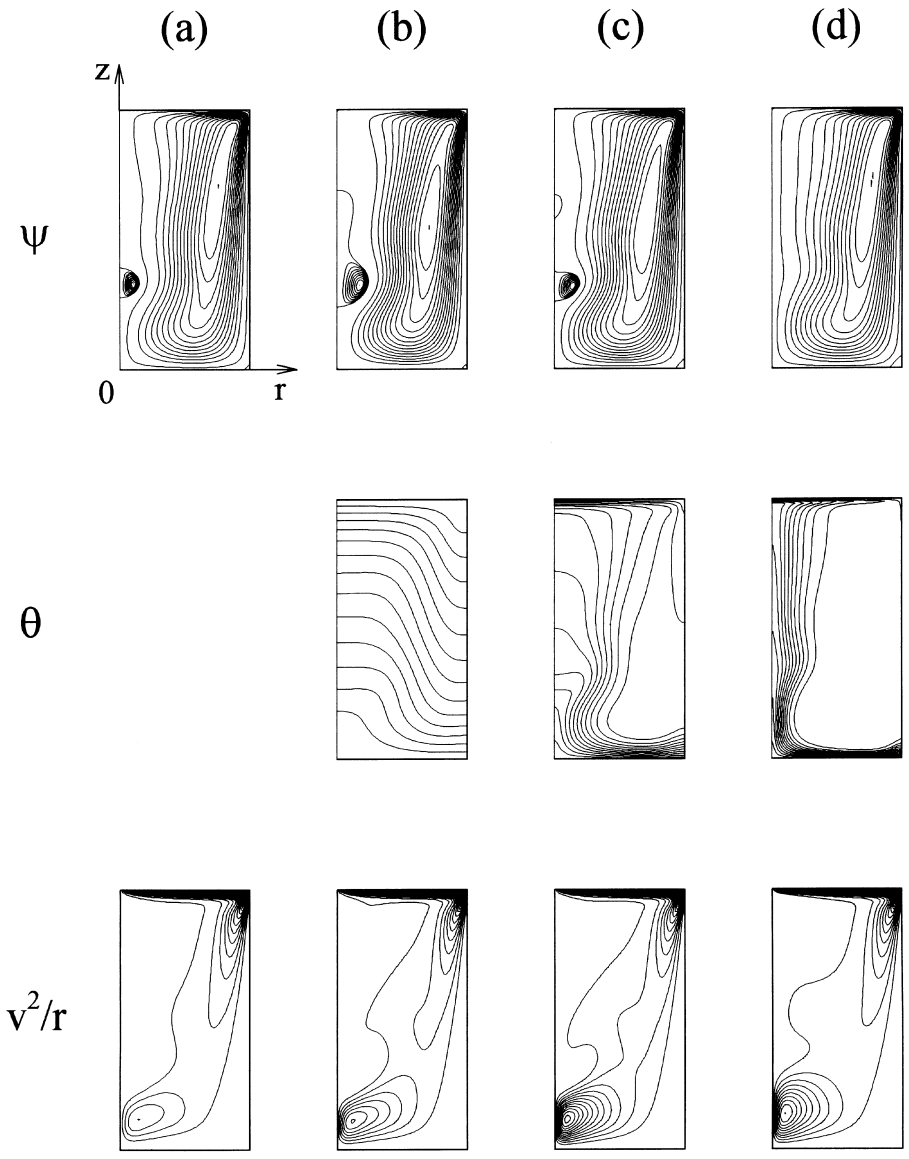

Fig. 2. Plots of ψ, θ, v^2/r in the meridonal plane for gravitationally unstable configuration. Conditions are $\mathrm{Re}=1600$ and $A=2.0$. The contour increments are $\Delta\psi=6.23\times10^{-4}$, $\Delta\theta=7.14\times10^{-2}$ and $\Delta(v^2/r)=0.01$. (a) Homogeneous fluid [$\mathrm{Ri}=0$]; (b) $\mathrm{Pr}=0.1$, $\mathrm{Ri}=-0.01$; (c) $\mathrm{Pr}=1.0$, $\mathrm{Ri}=-0.01$; (d) $\mathrm{Pr}=10.0$, $\mathrm{Ri}=-0.01$. The maximum and minimum values of ψ are: (a) $\psi_{\max}=1.34\times10^{-5}$, $\psi_{\min}=-8.22\times10^{-3}$; (b) $\psi_{\max}=1.08\times10^{-4}$, $\psi_{\min}=-9.34\times10^{-3}$; (c) $\psi_{\max}=5.64\times10^{-5}$, $\psi_{\min}=-8.94\times10^{-3}$; (e) $\psi_{\max}=5.62\times10^{-6}$, $\psi_{\min}=-8.23\times10^{-3}$. The maximum values of θ and v^2/r are 1.0 and the minimum values of θ and v^2/r are 0 for all the cases.

should be pointed out that the role of the azimuthal velocity shear term is crucial in bringing forth negative values of η. Also, the viscous effect is not entirely negligible in the localized region of stagnation bubble.

For a gravitationally unstable configuration with small Pr, the buoyancy effect (IV) is minor, and balance is maintained between (I) and (II), which is qualitatively akin to the homogeneous-fluid case. As is discernible in Fig. 2(b), $\partial\theta/\partial r$ is very weak at small radii for this case. However, it is noted that the magnitude of (II) is larger than for the homogeneous-fluid case. Clearly, since the overall stratification is unstable, the meridional motions are intensified in general, which leads to a vigorous azimuthal velocity and to a strengthened azimuthal velocity shear. This trend becomes more distinct as Pr grows to O(1) [see Fig. 4(d) for $\mathrm{Pr}=10.0$]. The buoyancy effect (IV) becomes appreciable, and, the role of (IV) is to produce positive values of η. This implies that the occurrence of stagnation bubble, i.e., vortex breakdown, is opposed by the buoyancy effect in this case. As is apparent in the temperature–field plot of Fig. 2(d), the isotherms are mostly parallel and vertical at small radii in the interior. Therefore, in this region, vertical buoyancy is weak, which discourages noticeable invigorations of meridional flows. In summary, it is argued that the disappearance of vortex breakdown bubble for large Pr, which was reported previously by Lugt and Abboud (1987) as well, can be explained by the tendency of the buoyancy term (IV) to oppose the generation of negative values of η near the axis.

3.2. Under a gravitationally stable temperature contrast ($Ri > 0$).

The numerical results for a gravitationally stable configuration, i.e., when $T_T > T_L$, are exemplified in Figs. 5–8 for $\mathrm{Re}=1600$ and $A=2.0$.

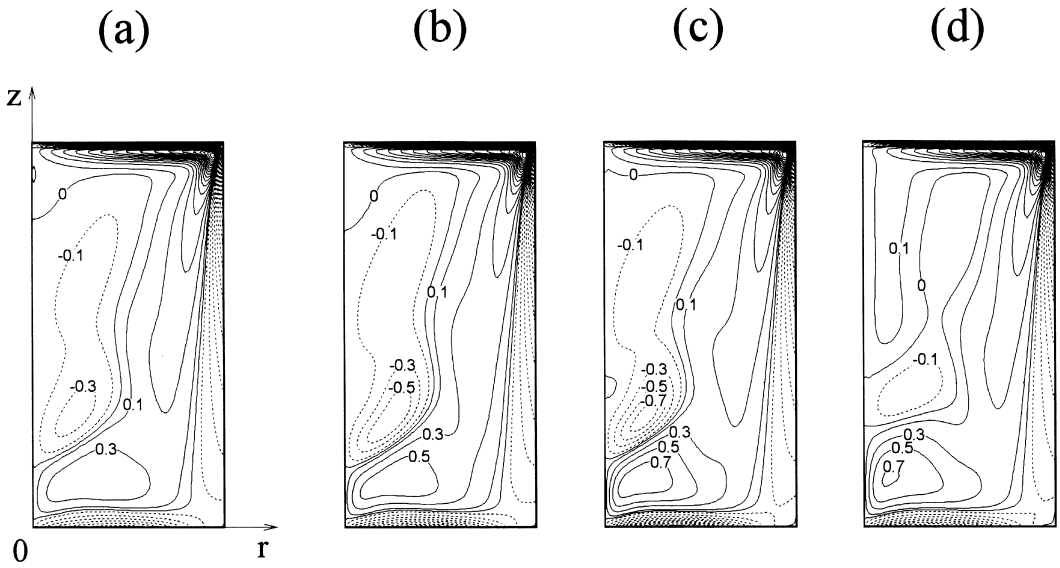

Fig. 3. Contour plots of azimuthal vorticity, η, in the meridional plane. Conditions are the same as in Fig. 2. Negative values of η are shown in dotted lines.

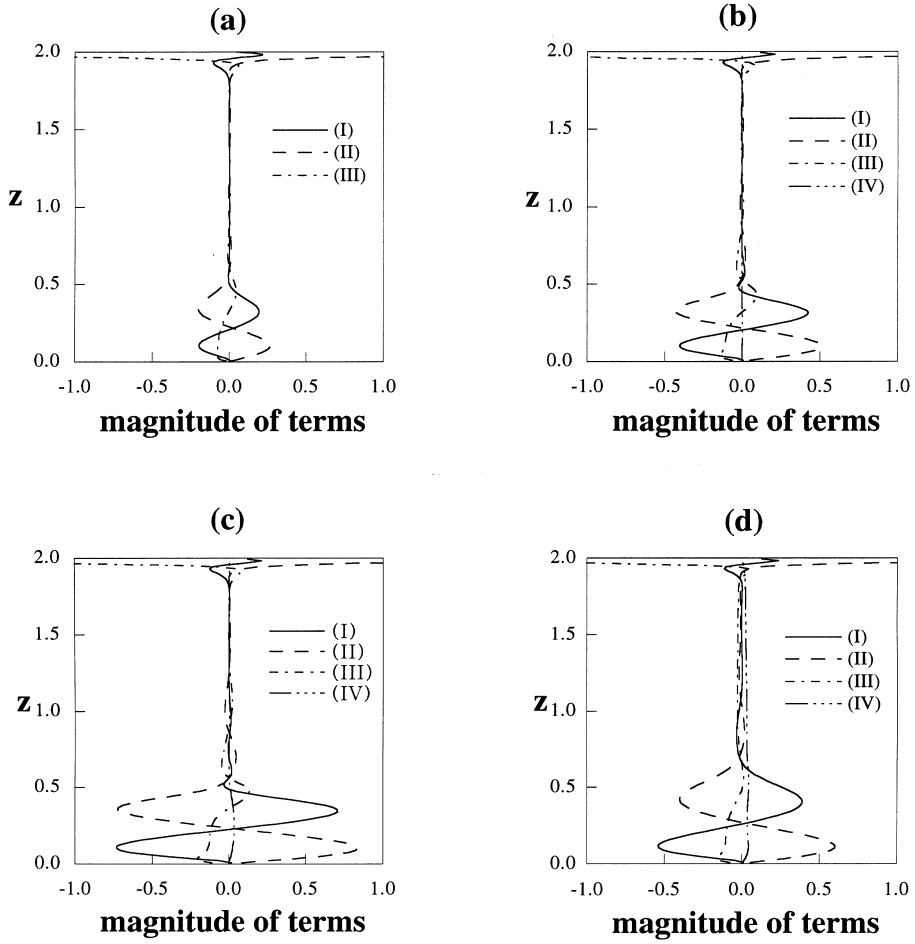

Fig. 4. Comparisons of the terms in the vorticity equation (2) along $r = 0.1$. Conditions are the same as in Fig. 2.

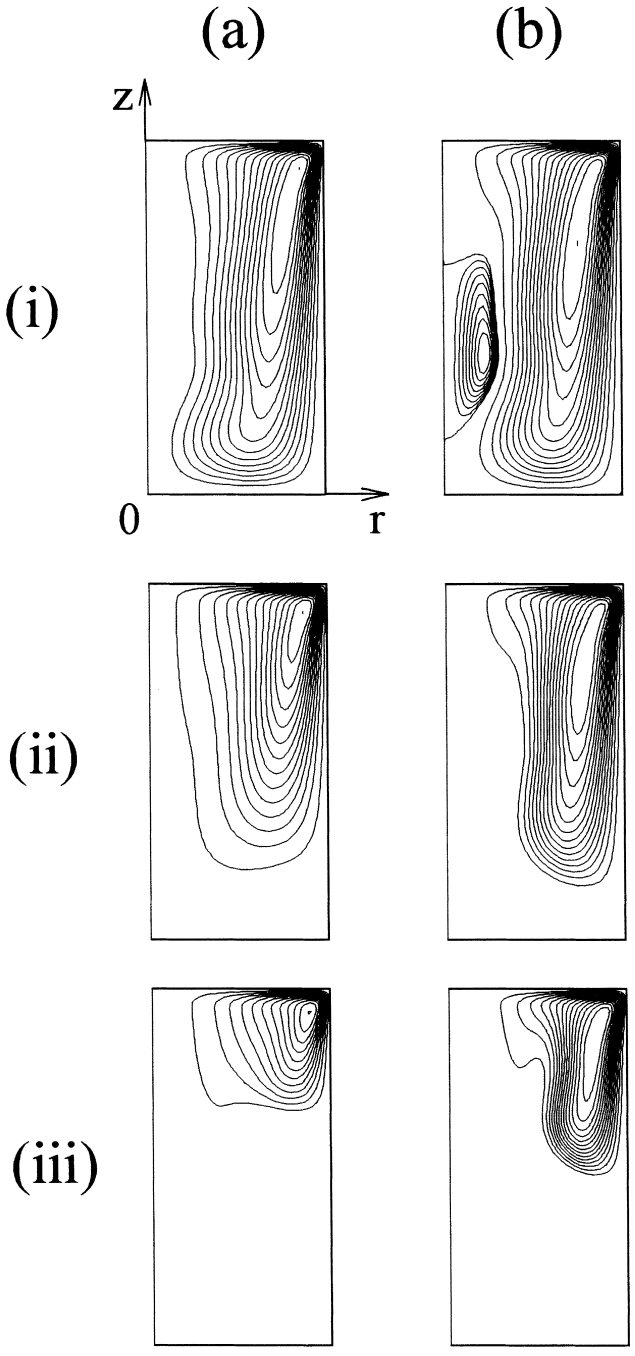

Fig. 5. ψ-Fields for gravitationally stable configuration. Conditions are $\mathrm{Re}=1600$, $A=2.0$. The contour increment is $\Delta\psi=5.70\times10^{-4}$. Values of Pr for the columns are: (a) $\mathrm{Pr}=0.1$; (b) $\mathrm{Pr}=10.0$; values of Ri for the rows are: (i) $\mathrm{Ri}=0.01$; (ii) $\mathrm{Ri}=0.1$; (iii) $\mathrm{Ri}=1.0$. The maximum and minimum values of ψ are: (a): (i) $\psi_{\max}=9.54\times10^{-8}$, $\psi_{\min}=-7.94\times10^{-3}$; (ii) $\psi_{\max}=1.18\times10^{-4}$, $\psi_{\min}=-7.64\times10^{-3}$; (iii) $\psi_{\max}=6.80\times10^{-4}$, $\psi_{\min}=-6.62\times10^{-3}$; (b): (i) $\psi_{\max}=1.61\times10^{-4}$, $\psi_{\min}=-8.31\times10^{-3}$; (ii) $\psi_{\max}=1.05\times10^{-4}$, $\psi_{\min}=-8.45\times10^{-3}$; (iii) $\psi_{\max}=1.75\times10^{-4}$, $\psi_{\min}=-8.51\times10^{-3}$.

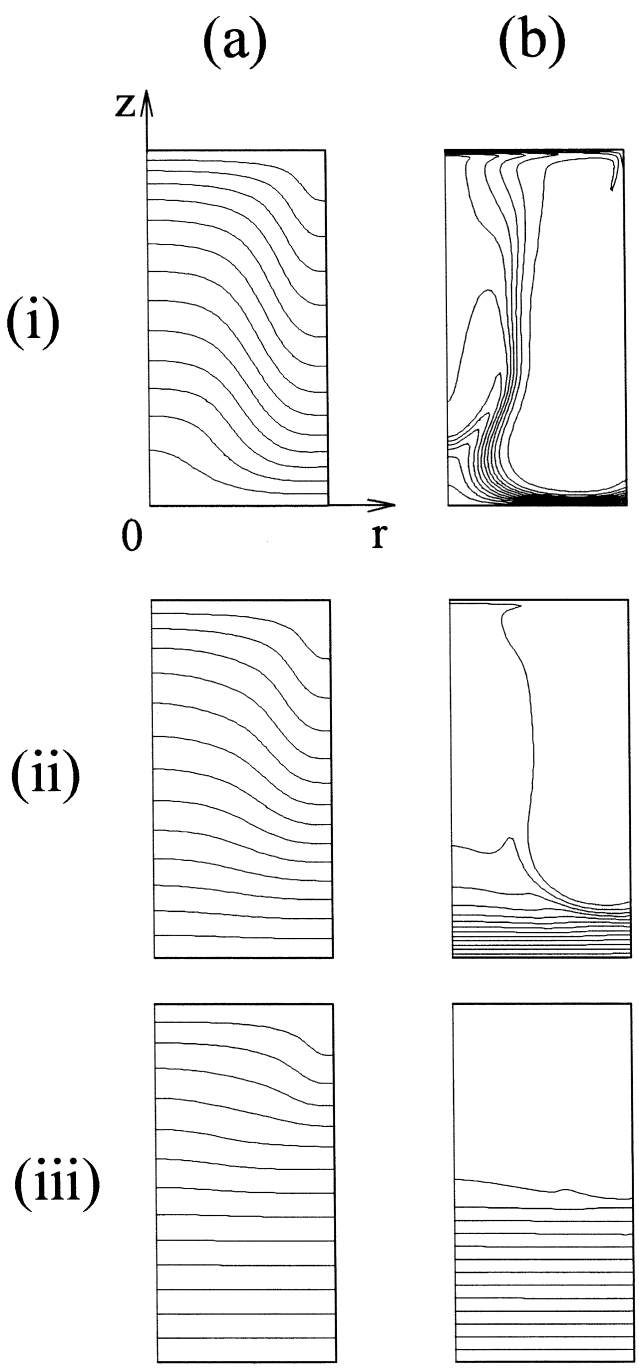

Fig. 6. θ-Fields for gravitationally stable configuration. Conditions are the same as in Fig. 5. The contour increment is $\Delta\theta=7.14\times10^{-2}$. $\theta_{\max}=1.0$ and $\theta_{\min}=0$ for all the cases.

First, frames (i) of Fig. 5 illustrate the meridional flow when Ri is small. Notice that, for $\mathrm{Pr}\ll1$ [see frame (a) (i) of Fig. 5], no stagnation bubble is seen. For $\mathrm{Pr}\sim\mathrm{O}(1)$, a distinct bubble is discernible on the axis, and the size of the bubble is larger for $\mathrm{Pr}>\mathrm{O}(1)$. It is recalled that these qualitative features are opposite to the case of $\mathrm{Ri}<0$. As the magnitude of Ri increases, the suppression of vertical motions becomes more effective, and the meridional flows tend to be concentrated to the upper portion of the cylinder. These characteristics are manifested in Fig. 5, and this reconfirms the earlier findings of Kim and Hyun (1997). Due to the inhibition of vertical flows, the formation of the stagnation bubble is discouraged, as demonstrated in Fig. 5.

Fig. 6 depicts the temperature field. Obviously, when $\mathrm{Pr}\ll1$, the dominance of conduction is apparent, and the isotherms show a tendency leading to a vertically linear dis-

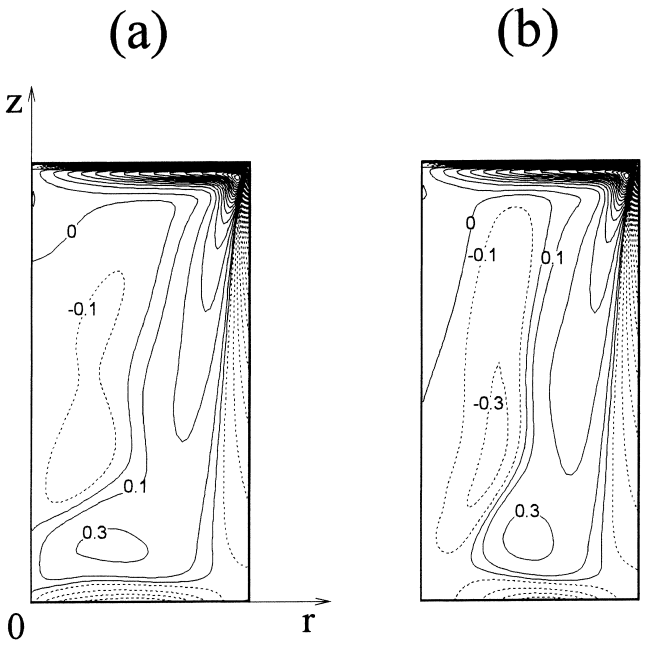

Fig. 7. Contour plots of azimuthal vorticity, η, in the meridional plane. Conditions are $\mathrm{Re}=1600$, $A=2.0$, $\mathrm{Ri}=0.01$. (a) $\mathrm{Pr}=0.1$; (b) $\mathrm{Pr}=10.0$.

tribution. This trend is more pronounced under a strong stable stratification, as displayed in frame (a) (iii) of Fig. 6. When $\mathrm{Pr} \gg 1$, the influence of convection prevails, which produces regions of nearly-uniform temperature in which convective activities are substantial.

Following the preceding assertions of Brown and Lopez, plots of azimuthal vorticity η are presented in Fig. 7 for $\mathrm{Ri}=0.01$. It is recalled that, as shown in Fig. 5, a stagnation bubble appears for $\mathrm{Ri}=0.01$ and no bubble is seen for $\mathrm{Ri} \gtrsim \mathrm{O}(1)$ for these flow conditions. Fig. 7 clearly exhibits that large negative values of η are found in broader regions for the case when a bubble exists.

This observation suggests that the kinematics-based argument of Brown and Lopez is qualitatively applicable to the present problem, which predicts the dynamic environment favorable for the formation of vortex breakdown bubble.

In an effort to examine the dynamical elements leading to negative values of η, Fig. 8 shows the term-by-term comparisons of the azimuthal vorticity equation (2). When $\mathrm{Pr} \ll 1$ [see Fig. 8(b)], the buoyancy term (IV) is negligible due to the smallness of horizontal temperature gradient. Also, the azimuthal-velocity shear term (II) is insignificant compared to the case of a homogeneous fluid [see Fig. 8(a)]. However, for $\mathrm{Pr} \gtrsim \mathrm{O}(1)$, the principal balance is maintained among the azimuthal-velocity shear term (II), nonlinear advection (I) and the buoyancy (IV). It is noted that the role of buoyancy (IV) is to generate negative η. Compiling these detailed observations, the

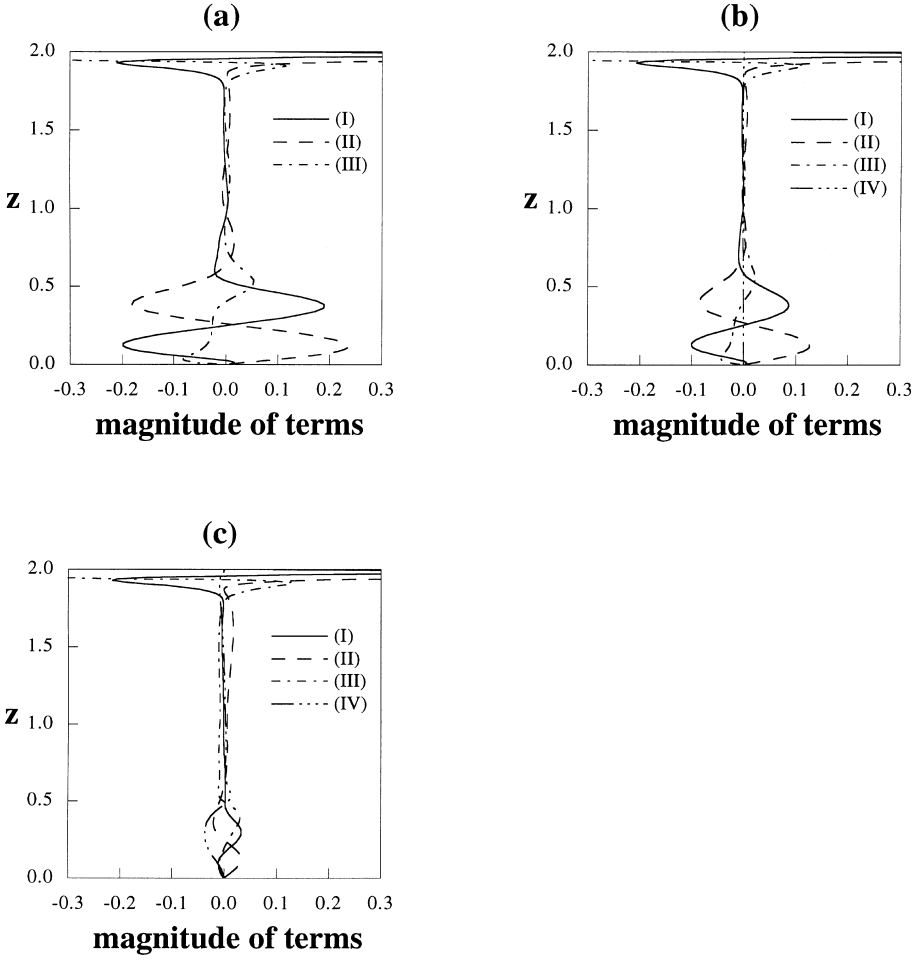

Fig. 8. Comparisons of the terms in the azimuthal vorticity equation (2) along $r=0.2$. Conditions are $\mathrm{Re}=1600$, $A=2.0$. (a) Homogeneous fluid [$\mathrm{Ri}=0$]; (b) $\mathrm{Pr}=0.1$, $\mathrm{Ri}=0.01$; (c) $\mathrm{Pr}=10.0$, $\mathrm{Ri}=0.01$.

major sources for the generation of negative η stem from the horizontal temperature-gradient (IV) and the azimuthal-velocity shear (II). It should be recalled that, for the case of $Ri < 0$, the role of horizontal temperature-gradient was to oppose the generation of negative η. For that case, negative η was achieved mainly by the azimuthal-velocity shear term.

In summary, the thrust of the present computational endeavors has been given in exploring the mechanism of occurrence of vortex breakdown. For a gravitationally-unstable configuration, the parameter ranges were similar to those of Lugt and Abboud (1987). Additional detailed information has been provided on the distributions of θ, v^2/r, η, and the budgets of individual terms of the azimuthal vorticity transport equation. For a gravitationally stable configuration, the analysis of Kim and Hyun (1997) was extended and modified by adding the above-stated results. In particular, emphasis was placed on the behavior of vortex breakdown bubble as Pr varied, which was not conducted previously.

4. Concluding remarks

The present numerical results demonstrate the significance of the behavior of azimuthal vorticity in predicting the occurrence of stagnation bubble. This is suggestive of the applicability of the inviscid, kinematics-based argument of Lopez (1990) and Brown and Lopez (1990) to the descriptions of flow of a stratified fluid, for both gravitationally unstable and gravitationally stable configurations.

By undergoing detailed comparisons of the terms comprising azimuthal vorticity equation, the relative importance of nonlinear advection, azimuthal velocity shear, viscous effects is assessed. When $Pr \ll 1$, the dominance of conduction is visible. Especially when $Ri > 0$, for Pr large, convection prevails, which produces regions of nearly-uniform temperature.

Experimental verifications of these flow processes involving a stratified fluid have not been reported in the literature. Plans are underway to embark on a systematic experimental program to supply visualizations which would exhibit the explicit influence of buoyancy in lid-driven rotating flows.

Acknowledgements

Appreciation is extended to the referees for constructive comments. This work was supported by grants from MOST, KOSEF and R&D Management Center for Energy Resources, South Korea.

References

Bertela, M., Gori, F., 1982. Laminar flow in cylindrical container with a rotating cover. Trans. ASME I: J. Fluids Eng. 104, 31–39.

Brown, G.L., Lopez, J.M., 1990. Axisymmetric vortex breakdown. Part 2. Physical mechanisms. J. Fluid Mech. 221, 553–576.

Brücker, Ch., Althaus, W., 1995. Study of vortex breakdown by particle tracking velocimetry(PTV). Pare 3: Time-dependent structure and development of breakdown-modes. Exp. fluids 18, 174–186.

Escudier, M.P., 1984. Observations of the flow produced in a cylindrical vessel with a rotating endwall. Exp. Fluids 2, 189–196.

Escudier, M.P., 1986. Vortex breakdown in technology and nature: and Vortex breakdown theories. Von Karman Institute for fluid dynamics Lecture Series Programme, 10, Introduction to vortex Dynamics, May 1986, Lectures 9 and 10.

Escudier, M.P., 1988. Vortex breakdown: Observations and Explanations. Prog. Aerospace Science 25, 189–229.

Hayase, T., Humphrey, J.A.C., Grief, R., 1994. A consistently formulated QUICK scheme for fast and stable convergence using finite-volume iterative calculation procedures. J. Comput. Phys. 98, 108–118.

Kim, W.N., Hyun, J.M., 1997. Convective heat transfer in a cylinder with a rotating lid under stable stratification. Int. J. Heat Fluid Flow 18, 384–388.

Lugt, H.J., Abboud, M., 1987. Axisymmetric vortex breakdown with and without temperature effects in a container with a rotating lid. J. Fluid Mech. 179, 179–200.

Lopez, J.M., 1990. Axisymmetric vortex breakdown. Part 1. Confined swirling flow. J. Fluid Mech. 221, 533–552.

Pao, H.P., 1970. A numerical computation of a confined rotating flow. Trans. ASME E: J. Appl. Mech. 37, 480–487.

Pao, H.P., 1972. Numerical solution of the Navier–Stokes equations for flows in the disk-cylinder system. Phys. Fluids. 15, 4–11.

Patankar, S.V. 1980. Numerical Heat Transfer and Fluid Flow. McGraw-Hill, New York.